

Environmental Science Advances

Accepted Manuscript

This article can be cited before page numbers have been issued, to do this please use: D. Mahapatra and D. Swain, *Environ. Sci.: Adv.*, 2026, DOI: 10.1039/D6VA00012F.



This is an Accepted Manuscript, which has been through the Royal Society of Chemistry peer review process and has been accepted for publication.

Accepted Manuscripts are published online shortly after acceptance, before technical editing, formatting and proof reading. Using this free service, authors can make their results available to the community, in citable form, before we publish the edited article. We will replace this Accepted Manuscript with the edited and formatted Advance Article as soon as it is available.

You can find more information about Accepted Manuscripts in the [Information for Authors](#).

Please note that technical editing may introduce minor changes to the text and/or graphics, which may alter content. The journal's standard [Terms & Conditions](#) and the [Ethical guidelines](#) still apply. In no event shall the Royal Society of Chemistry be held responsible for any errors or omissions in this Accepted Manuscript or any consequences arising from the use of any information it contains.

Environmental Significance Statement

View Article Online
DOI: 10.1039/D6VA00012F

Rapid urbanization has driven extensive infrastructure growth and industrialization, leading to conversion of vegetated land to impervious surfaces. This transformation intensifies land surface temperature (LST) extremes, disrupting surface energy balance, exacerbating climate extremes, and increasing public health risks. This study evaluates evolving land surface thermal hotspots in the tropical state of Odisha, India, using high-resolution satellite based LST retrievals. Results show that built-up areas exhibit significantly higher hotspot intensities than non-built-up regions. Districts experiencing rapid population growth and industrial expansion demonstrate increases in thermal hotspots, reaching rates of up to 9% per year and for Coastal districts ranging from 2% to 9% over seven years. These findings underscore the dominant role of impervious surfaces in regulating surface thermal regimes and also demonstrate the potential for a priori hotspot detection to support proactive and location-specific mitigation strategies.



1 **Rising urban Land Surface Thermal Extremes in a rapidly evolving tropical Indian State**

2 Dikshika Mahapatra and Debadatta Swain*

3 School of Earth, Ocean and Climate Sciences, Indian Institute of Technology Bhubaneswar, Argul, Jatni, Odisha,
4 India, 752050.

Open Access Article. Published on 28 May 2026. Downloaded on 5/30/2026 1:10:57 PM.
This article is licensed under a Creative Commons Attribution-NonCommercial 3.0 Unported Licence.



5
6
7
8
9
10
11
12
13
14
15
16
17
18
19
20
21
22
23 *Corresponding Author (Email: dswain@iitbbs.ac.in)

25 Abstract

26 India, as a developing country is undergoing accelerated urbanization. However, this rapid and often unplanned urban
27 growth has become a major concern as it significantly alters land surface characteristics. This leads to increased land
28 surface temperatures (LST) which contributes to deteriorating air quality, energy overconsumption, and adverse health
29 conditions, posing substantial challenges to sustainable urban climate management. The current study focuses on the
30 identification and analysis of the evolution of thermal hotspots across 30 districts of Odisha, a rapidly developing
31 tropical Indian state utilizing 20 years of datasets from Moderate Resolution Imaging Spectroradiometer (MODIS)
32 onboard Terra and Aqua, and Sentinel-2 satellite missions for the pre-monsoon season during 2017 to 2023. The
33 analysis revealed that built-up areas exhibited significantly higher hotspot intensities than non-built-up regions.
34 Districts with rapid population and industrial growth with extensive impervious surfaces and reduced vegetation
35 showed a marked rise in thermal hotspots (at a maximum rate of 9% per year) emphasizing the role of impervious
36 surfaces in modulating surface temperatures. In contrast, percentage of hotspots coverage was higher over non-built-
37 up areas for predominantly agrarian and semi-arid districts, likely due to the progressive decrease in vegetation cover
38 from anthropogenic activity and consequent exposure of bare land. Further, analysis indicated an intense prevalence
39 of hotspots in rapidly urbanizing coastal districts with a minimum (maximum) rise of 2% (9%) area of hotspots in just
40 seven years. These findings highlight the critical need for targeted mitigation strategies in urban areas facing
41 intensified thermal stress.

42
43 **Keywords:** Thermal Hotspots; Land Surface Temperature; Urbanization, MODIS, Sentinel-2



44 1. Introduction

45 The increasing population and anthropogenic activities in rapidly developing countries have significantly impacted
46 different natural land covers and associated surface properties.¹⁻³ Rapid infrastructure development and
47 industrialization to accommodate the pressing needs of a fast-growing population are among the major factors
48 affecting thermal comfort in urbanized cities.⁴ Consequently, the land cover gets converted from vegetation to
49 impervious surfaces like concrete, asphalt, and buildings, which retain more heat.⁵⁻⁷ Hence, land use land cover
50 (LULC) change is deemed as one of the major causes of rising Land Surface Temperatures (LST) in urban areas.⁸⁻¹⁰
51 This also leads to the Urban Heat Island (UHI) effect, which highlights the difference in temperature between the
52 urban region and its surrounding rural regions.¹¹⁻¹³ The regions associated with very high LSTs contribute to the
53 climate extremities, anomalous radiation budget, and significant environmental damages as well a health hazards.¹⁴
54 The prevalence of these thermal hotspots directly translates into a degradation of urban environmental quality and
55 poses significant risks to public health. Several studies have shown increasing LSTs to have a close correlation with
56 air temperatures leading to elevated thermal exposure in urban regions^{15,16} with the most immediate consequence of
57 severe reduction in thermal comfort; and persistent high temperatures creating conditions of heat stress for urban
58 dwellers.¹⁷ Indirectly, higher environmental temperatures could contribute to poorer air quality by accelerating the
59 chemical reactions that form harmful ground-level ozone as well as increasing surface convection. This in turn could
60 be a potent respiratory irritant, thereby creating a compounding public health challenge.^{18,19} In addition, prolonged
61 exposure to extreme heat, especially within these hotspots, elevates the risk of heat-related illnesses such as heat
62 exhaustion, heat cramps, and life-threatening heatstroke.^{20,21} The elevated thermal load can also exacerbate pre-
63 existing chronic conditions, placing a dangerous strain on the cardiovascular and respiratory systems of vulnerable
64 populations, including the elderly, children, and individuals with heart or lung disease.^{18,22} Consequently, a detailed
65 and precise identification of these high-temperature zones is essential for developing targeted mitigation of public
66 health hazards and enhance urban habitability.

67
68 Most of the earlier studies on LST variability and trends generally focused on the analysis of average LST changes
69 over a region, which lacked the identification of localized effects.²³ Satellite-based thermal sensors are useful in
70 identifying the “Thermal Hotspots” on the ground, which are regions showing consistently higher temperatures as
71 compared to their surroundings.²⁴⁻²⁷ The escalating challenge of thermal hotspot formation in dense tropical and



72 mediterranean built-up areas is increasingly tied to the nonlinear expansion of impervious surfaces. Recent research
73 in megacities like Shanghai demonstrated that LST does not rise linearly with urbanization, and a critical threshold
74 exists at approximately 40% impervious cover, beyond which heat accumulation intensifies disproportionately.²⁸ This
75 phenomenon is exacerbated in semi-arid cities, where the conversion of vacant land to built-up infrastructure has
76 created persistent thermal islands over the last decade.²⁹ In these environments, core urban zones frequently exhibited
77 temperatures 4°C to 5°C higher than their rural counterparts, a trend particularly evident in Mediterranean climates,
78 where residential hotspots accounted for 11% of the urban fabric.³⁰ The thermal hotspot occurrences are especially
79 complicated by the spatiotemporal dynamics of coupled urban-thermal-ecological interactions, as seen in the western
80 Himalayan foothills, where indices like the Normalized Difference Built-up Index (NDBI) and Bare Soil Index (BSI)
81 showed strong positive correlations with LST, reaching coefficients as high as 0.78 and 0.82, respectively.³¹ Moreover,
82 the impact of these hotspots extended beyond environmental discomfort to economic consequences, as in Tehran,
83 surface urban heat islands (SUHI) have been found to elevate urban temperatures by 5°C to 12°C, subsequently
84 increasing annual building cooling energy demands by 15–20%.³² Recent methodological shifts to local-scale
85 microclimatic assessments emphasized the need for high-resolution, small-scale investigations to assess the true
86 mitigation potential of nature-based solutions and policies.^{33,34} Furthermore, the integration of multi-sensor data,
87 including the use of Landsat-9 and Sentinel-2, allowed for a more granular identification of these thermal anomalies
88 in recent times, ensuring that urban planning interventions could be directed toward the most vulnerable built-up
89 sectors.^{28,30}

91 A wide range of remote sensing sensors like Thematic Mapper (Landsat 4 & 5), Enhanced Thematic Mapper+ (Landsat
92 7), Thermal Infra-Red Sensor (Landsat 8 & 9), Moderate Resolution Imaging Spectroradiometer (MODIS onboard
93 Terra and Aqua), Advanced Very High-Resolution Radiometer (AVHRR onboard MetOp), Advanced Spaceborne
94 Thermal Emission and Reflection (ASTER onboard Terra) are currently being utilized for obtaining LST. But,
95 resolving rapid variations of LST over the highly heterogeneous land surfaces from coarse-resolution (30 m and above)
96 satellite images still remains a challenge. This arises due to the satellite orbital constraints, creating a trade-off between
97 their spatial and temporal resolutions.³⁵ To overcome this limitation, various studies have utilized downscaling
98 techniques to generate LST data with high spatial as well as temporal resolutions.^{36,37} Different approaches are used
99 by researchers for the LST downscaling, like the DisTrad (Disaggregation of Radiometric Temperature) method,



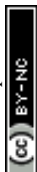
100 which is based on the linear relationship between LST and NDVI.³⁸ This is further modified as TsHARP (Temperature
101 Sharpening), which considers NDVI as a regression kernel. Statistical regression-based methods like linear,
102 multilinear, and non-linear approaches were widely used.^{39,40} However, vegetation parameters alone cannot describe
103 the LST variability in a complex terrain system. Along with NDVI, Normalized Difference Builtup Index (NDBI),
104 Normalized Difference Bareness Index (NDBaI) are also some of the major factors related to LST in an urban
105 region.⁴¹⁻⁴³ The current study is designed to identify the thermal hotspots by retrieving high-resolution LST over highly
106 heterogeneous landscapes which are prone to the impacts of heat stress. Attempt is also made to demonstrate a-priori
107 detection of thermal hotspots which could contribute to expedite targeted mitigation strategies.

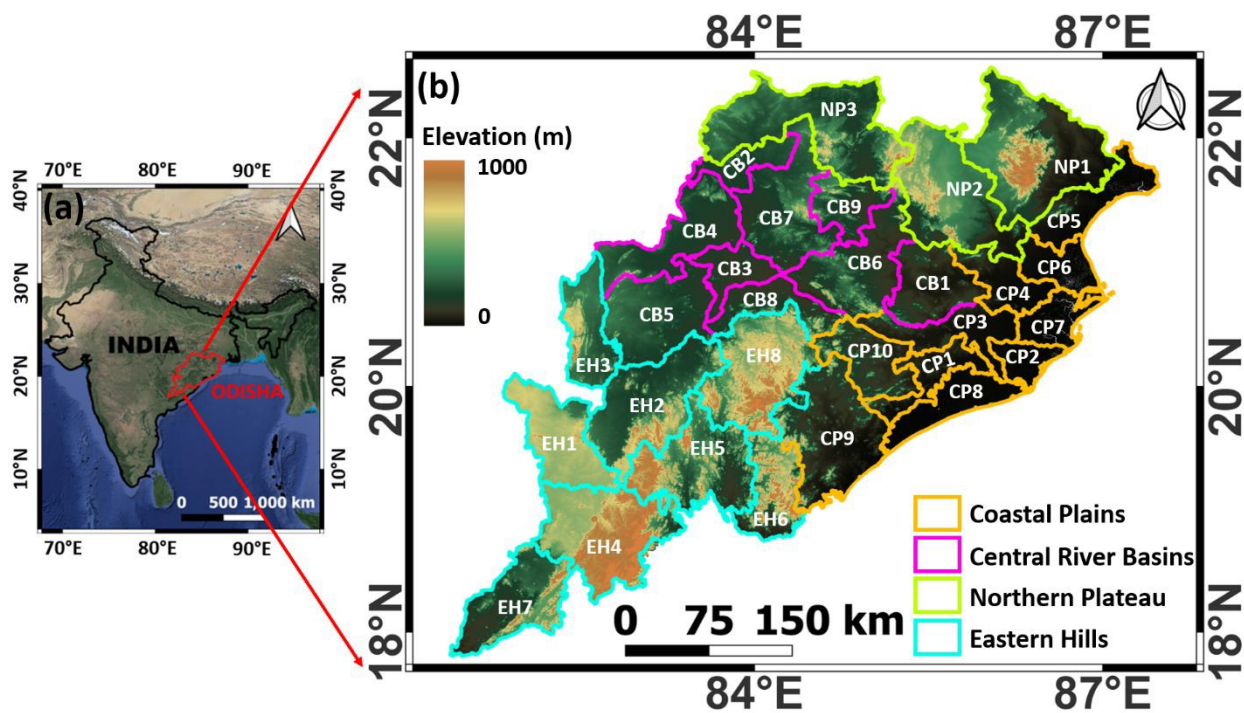
109 2. Study area, data, and methodology

110 2.1 Study area

111 The study focused on Odisha covering approximately 155,707 square kilometers, located on the eastern coast of India,
112 between latitudes 17.78° N to 22.73° N and longitudes 81.37° E to 87.53° E (Figure 1a). The state shares a 570 km
113 coastal boundary with the Bay of Bengal to the east and land-locked on the other three sides. The state also
114 harbours diverse topographical features, ranging from coastal plains to mountainous and plateaus. Odisha experiences
115 a tropical climate characterized by hot summers, mild winters, and a monsoon season. This region has historically
116 been a disaster and disease-prone area, with an abundance of vector-borne diseases like malaria, dengue, and Japanese
117 encephalitis.⁴⁴ The state has emerged as a hub of major urban-industrial complexes in recent times, which has
118 potentially increased the possible spread of such health hazards. The state of Odisha is broadly divided into four major
119 geographical regions, namely Coastal Plains (CP), Central River Basins (CB), Northern Plateau (NP) and Eastern
120 Hills (EH), as marked in Figure 1b⁴⁵. The districts are categorized as per these zones and numbered in the order of
121 their population densities of 2011 Census (Table 1).⁴⁶ Figure 1b and Table 1 also represent the elevation map of
122 Odisha and the mean elevation of the 30 districts, as calculated from the NASA – Shuttle Radar Topography Mission
123 Digital Elevation Model (SRTM DEM) available for the year 2000, respectively.⁴⁷ Khordha district was observed to
124 have the highest population density, being the most urbanized district and Bhubaneswar city, the capital of the state.
125 Kandhamal, which consists of dense forests and hills, had the lowest population density. Out of the 30 districts,
126 Koraput is situated at the highest elevation while Kendrapara is at the lowest elevation above mean sea level.

127





128
129 **Fig. 1** (a) Location of Odisha, (b) District-level map (segregated into four geographical regions and numbered as per
130 their population densities in 2011), along with the SRTM elevation data as the background

Open Access Article. Published on 28 May 2026. Downloaded on 5/30/2026 1:10:57 PM.
This article is licensed under a Creative Commons Attribution-NonCommercial 3.0 Unported Licence.



Environmental Science: Advances Accepted Manuscript

132 **Table 1** Demography of the 30 districts of Odisha in 2011 as per the Census⁴⁶, and their mean elevation (metres
133 above mean sea level)

Sl. No.	Name	Population Density (per km ²)	Elevation (m)	Sl. No.	Name	Population Density (per km ²)	Elevation (m)
CP1	Khordha	800.45	58.5	EH1	Nabarangpur	230.76	596.1
CP2	Jagatsinghpur	681.64	7.6	EH2	Kalahandi	199.09	376.7
CP3	Cuttack	667.46	65.1	EH3	Nuapada	158.45	382.3
CP4	Jajpur	630.28	53.3	EH4	Koraput	156.65	753.4
CP5	Baleswar	609.71	31.8	EH5	Rayagada	136.85	482.6
CP6	Bhadrak	601.33	9.9	EH6	Gajapati	133.59	520.1
CP7	Kendrapara	544.77	4.7	EH7	Malkangiri	105.88	336.1
CP8	Puri	488.28	6.8	EH8	Kandhamal	91.39	626.0
CP9	Ganjam	430.05	149.8	NP1	Mayurbhanj	241.86	308.2
CP10	Nayagarh	247.51	177.6	NP2	Keonjhar	216.99	376.5
CB1	Dhenkanal	275.79	113.1	NP3	Sundargarh	215.55	319.9
CB2	Jharsuguda	274.13	222.4				
CB3	Sonepur	261.09	141.6		Prefix	Geographical Region	
CB4	Baragarh	253.77	226.3		CP:	Coastal Plains	
CB5	Balangir	250.79	240.6		CB:	Central River Basins	
CB6	Angul	199.81	214.8		EH:	Eastern Hills	
CB7	Sambalpur	157.17	260.0		NP:	Northern Plateau	
CB8	Boudh	142.40	208.9				
CB9	Deogarh	106.29	249.1				

Districts in each zone are sorted based on their population density

134

135 2.2 Data

136 Thermal hotspots play a crucial role in modulating the thermal comfort of a region. The peak thermal characteristics
137 of the land surface are usually observed in the afternoon^{48,49}, whereas high-resolution satellite imagery is available in
138 the morning only over the Indian region (local pass time at around 10:30 hrs IST). Hence, the need for a high-resolution
139 afternoon-time LST dataset to accurately identify urban thermal hotspots. For the analysis, Sentinel-2 surface
140 reflectance data sets at 10:30 am IST available at 10 m spatial resolution and 5 days' temporal resolution were obtained
141 from the Copernicus Open Access Hub (scihub.copernicus.eu/) for the pre-monsoon period spanning the years 2017
142 to 2023. Additionally, Sentinel-2 LULC data were obtained from ESRI Living Atlas repository
143 (livingatlas.arcgis.com) for the analysis period. Surface reflectance and LST data products from MODIS-Terra



144 (MOD09A1.061 for reflectance) at 10:30 IST and MODIS-Aqua (MYD09A1.061 for reflectance and MYD11A2.061
 145 for LST) at 13:30 IST (afternoon) at 1 km spatial resolution were also obtained from NASA LPDAAC
 146 (earthdata.nasa.gov/data) for the pre-monsoon period of 2004 to 2023. This study developed a multi-sensor approach,
 147 combining Sentinel-2 (high resolution, available only in the morning) and MODIS-Terra/Aqua (moderate resolution,
 148 available during both morning and afternoon) satellite data to detect LST hotspots. MODIS LSTs for the pre-monsoon
 149 period from 2004 to 2023 was utilized to establish a long-term climatological baseline for LST estimation, while
 150 MODIS and Sentinel-2 data sets for the period 2017 to 2023 were utilized for the detailed analysis. A selective
 151 validation of Sentinel-2 derived LST was attempted over one of the districts during the pre-monsoon period during
 152 2024 based on ground truth data availability. Yearly high-resolution population metrics for the 2017-2023 period were
 153 obtained from the WorldPop global population counts in 100 m × 100 m grids
 154 (<https://hub.worldpop.org/geodata/listing?id=135>) to investigate the risks owing to population density.

156 2.3 Methodology

157 The first step of the analysis involved computation of remote sensing indices from the available surface reflectances
 158 from MODIS and Sentinel-2. Normalized difference method was used to compute NDVI⁵⁰, NDBI⁵¹, NDBaI⁵² and
 159 NDMI⁵³ from appropriate spectral bands of the Sentinel-2 and MODIS, separately. These indices were then used in a
 160 two-stage regression formulation to obtain 10 m resolution LSTs at 13:30 hrs. First, a simple linear regression fit was
 161 established between MODIS morning and afternoon indices, using Eq. 1.

$$y = mx + c \quad (1)$$

162 where x , y denotes the morning and afternoon indices, while, m , and c represent the slope and intercepts, respectively.
 163 The resulting transfer functions were applied to morning Sentinel-2 indices, namely, NDVI, NDBI, NDBaI and NDMI
 164 to estimate afternoon indices at 10 m resolution. This was followed by the development of a multiple linear regression
 165 model relating MODIS-Aqua LSTs and indices, both available in the afternoon, using Eq. 2.

$$LST = m_1NDVI + m_2NDBI + m_3NDBaI + m_4NDMI + c \quad (2)$$

166 where m_1 , m_2 , m_3 , m_4 and c are estimated model coefficients. This relation was thereafter applied to the 10 m
 167 Sentinel-2 afternoon indices to obtain downscaled LSTs at 10 m for 30 districts of Odisha. A methodological
 168 validation of Sentinel-2 derived LSTs was also carried out against Aqua-MODIS LST observations. This particular
 169 MODIS product is known to be a widely accepted benchmark in satellite-based thermal studies.⁵⁴⁻⁵⁶ To enable direct



170 comparison, 10 m Sentinel-2 LST pixels were spatially averaged to match the 1 km MODIS grid. Using an area-
171 proportional stratified random sampling approach, widely used in geospatial comparisons,⁵⁷⁻⁵⁹ 3,234 MODIS pixels
172 were selected across the 30 districts and statistically compared with the corresponding 1 km-averaged Sentinel-2 pixels
173 of the same number. Further, the downscaled LST was validated against *in situ* observations for Khordha (CP1)
174 district of Odisha during 2nd March and 11th May 2024.

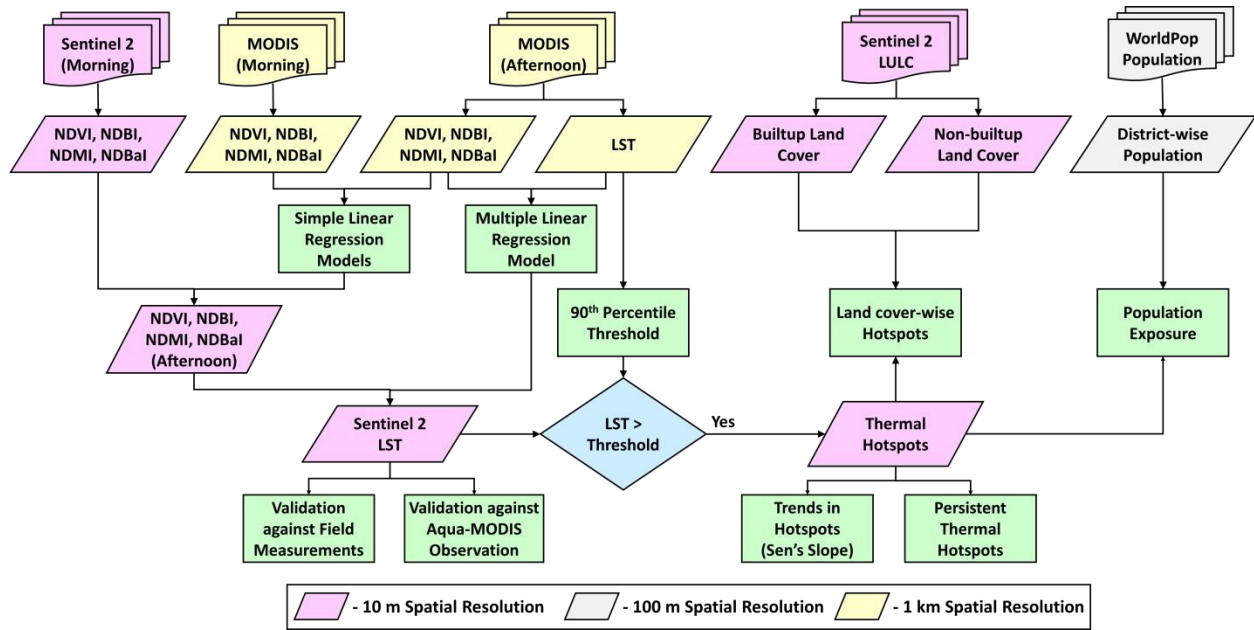
175
176 The next step involved identification of thermal hotspots in all the 30 districts. For this, a LST threshold value from
177 the afternoon MODIS LST 20-years climatology was computed for each pixel over the study region. The LST was
178 defined as the 90th percentile of the historical LST distribution.⁶⁰ This percentile-based approach ensures that a hotspot
179 is classified as an area experiencing significantly higher temperatures relative to its own long-term thermal variability.
180 The high-resolution LST derived from Sentinel-2 for the study period (2017-2023) was then compared against this
181 baseline, and any pixel with an LST value exceeding the threshold was designated as a thermal hotspot. Additionally,
182 Sentinel-2 LULC datasets were analysed to assess the influence of land cover change on hotspot occurrences during
183 the study period. The LULC classes were first categorised into built-up and non-built-up. The built-up class
184 encompassed impervious surfaces like urban infrastructure and industrial areas, while the non-built-up class consisted
185 all other land covers including vegetation, barren land, and agricultural fields. The total area and percentage area of
186 hotspots over the two classes were then estimated for all the districts during the period 2017 to 2023. Evolution of
187 thermal hotspots over time and the corresponding areas were quantified through trend analysis utilizing the Sen's
188 slope method. All statistical parameters presented in the current work were also examined for significance at a
189 confidence level of 95%. Persistent thermal hotspots (PTH) in all the districts were calculated by selecting the pixels
190 that showed higher temperatures above the threshold value (90th percentile) for more than half the study period.
191 Finally, population exposure was estimated as the number of persons exposed to thermal hotspots within a 100m ×
192 100m grid, calculated using Eq. 3. Since, Sentinel-2 LST was derived at 10 m resolution, the maximum number of
193 possible hotspot pixels in a 100m × 100m population grid was 100. Hence, the total population in a 100m × 100m grid
194 was multiplied with the fraction of hotspots in that grid to calculate the total number of persons exposed to hotspots,
195 assuming that the population distribution in that grid is homogeneous.⁶¹ Percentage population exposure was
196 calculated as the percentage of population of a district exposed to hotspots compared to its total population. Figure 2
197 summarizes the overall methodology of the current study.



198

$$Pop. Exp. = \frac{(No. of hotspot pixels)}{(No. of total pixels)} \times population \quad (3)$$

199



200

201

202

Fig. 2 Flowchart of the methodology.



203 3. Results and discussions

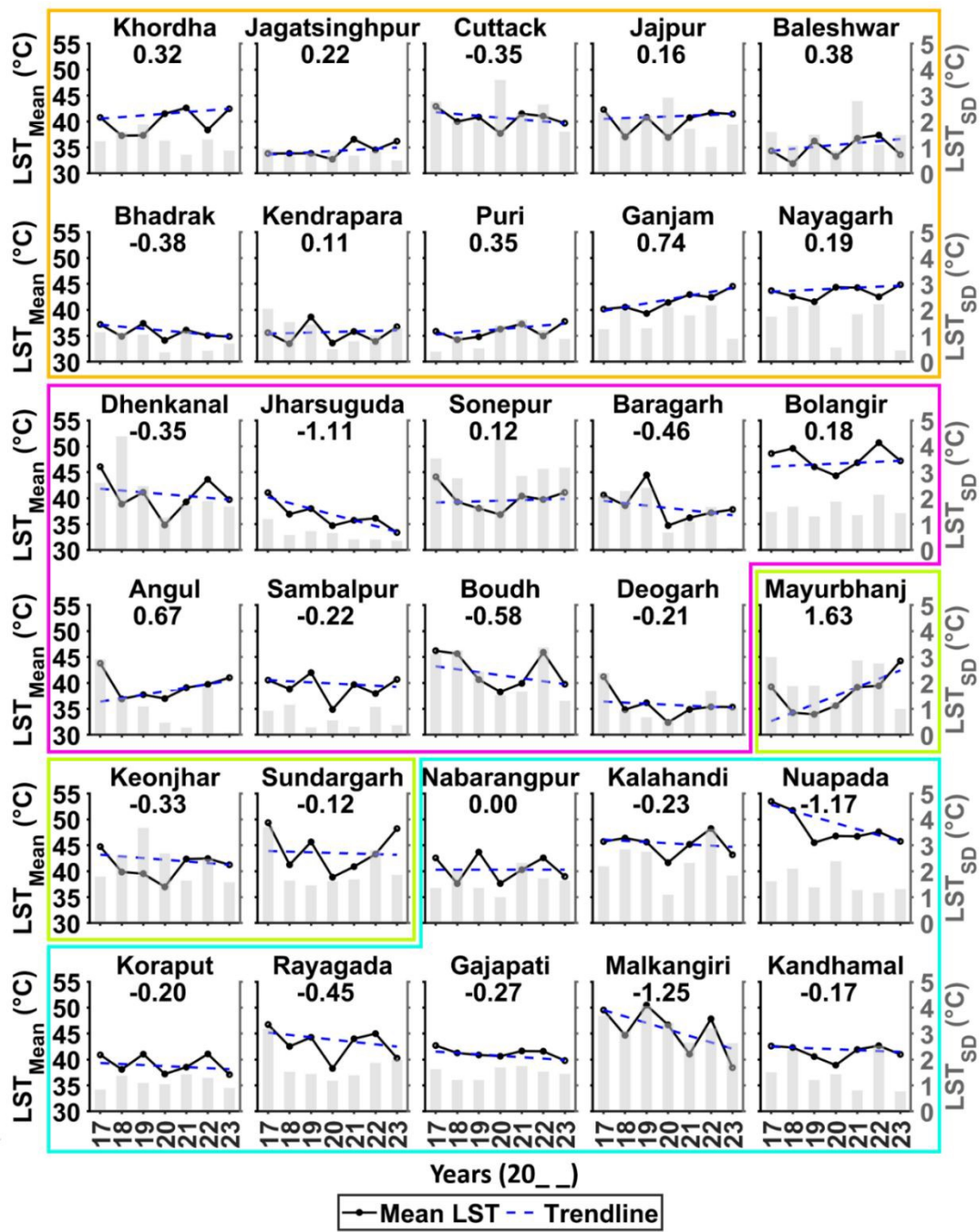
204 3.1 Thermal hotspots from downscaled LST

205 The downscaling approach combining Sentinel-2 and MODIS datasets was carried out to generate afternoon time LST
206 at 10 m resolution over the study area. The descriptive statistics of LST (LST_{Mean} and LST_{SD}) were first analyzed to
207 assess its spatio-temporal variations across the four zones of the study area, as presented in Figure 3. In the CP districts,
208 characterized by low altitude and high population density, a predominant warming trend (was observed, with districts
209 such as Ganjam (CP9), Baleswar (CP5), and the highly urbanized Khordha (CP1) showing positive LST trends.
210 However, exceptions included Cuttack (CP3) and Bhadrak (CP6), which exhibited cooling LST trends. Cuttack has a
211 unique geographical setting, a deltaic region bounded by two major rivers, Mahanadi and Kathajodi, on either side.
212 This proximity to large streams of flowing waters could possibly result in the cooling trends with water behaving as a
213 localized thermal buffer owing to its high specific heat capacity.⁶² Similarly, the cooling trends in Bhadrak could
214 largely be driven by the expansive agricultural land which would enhance evaporative cooling through transpiration
215 and close proximity to the Bay of Bengal sharing its boundary with the ocean.⁶³

216
217 Moving to the CB districts, the trends were highly heterogeneous (Figure 3). While Angul (CB6) exhibited a
218 significant warming trend, likely due to industrial activity, Jharsuguda (CB2) displayed a sharp decline in mean LST,
219 suggesting localized cooling factors or changes in land cover. The NP districts were defined by a striking contrast,
220 where Mayurbhanj (NP1) exhibited the highest warming rate across the entire state, drastically diverging from its
221 zonal counterparts, Keonjhar (NP2) and Sundargarh (NP3), which showed slight cooling. Conversely, the EH districts,
222 situated at higher altitudes, displayed a consistent cooling trajectory across almost all districts, with Malkangiri (EH8)
223 and Nuapada (EH3) recording the most substantial negative slopes, indicating that the high-altitude distinct geography
224 may be experiencing a temperature stabilization or reduction compared to the warming signals observed in the lower-
225 elevation, densely populated coastal and industrial districts. The standard deviation (grey bars) fluctuated annually
226 throughout the districts, indicating inter-annual variability in temperature extremes. These often peaked in the years
227 like 2019 or 2022, depending on the specific zone. LST_{SD} was lower in CP districts as compared to the other zones.
228 The distinct spatial pattern of such LST variations was likely driven by the moderating maritime influence of the Bay
229 of Bengal, which provided a cooling and stabilizing effect to coastal districts.⁶⁴ Inland regions, lacking this effect and
230 potentially influenced by local topography and land cover, experienced a stronger continental climate with more



231 extreme heat.⁶⁵ Furthermore, the influence of urban morphology, such as increased shading in high-density and high-
 232 rise residential clusters, could contribute to lower surface temperatures compared to the expansive industrial
 233 surfaces.⁶⁶ These findings underscored the fact that while urbanization typically drives warming, local environmental
 234 and morphological factors can effectively modulate its intensity and extent.
 235



236

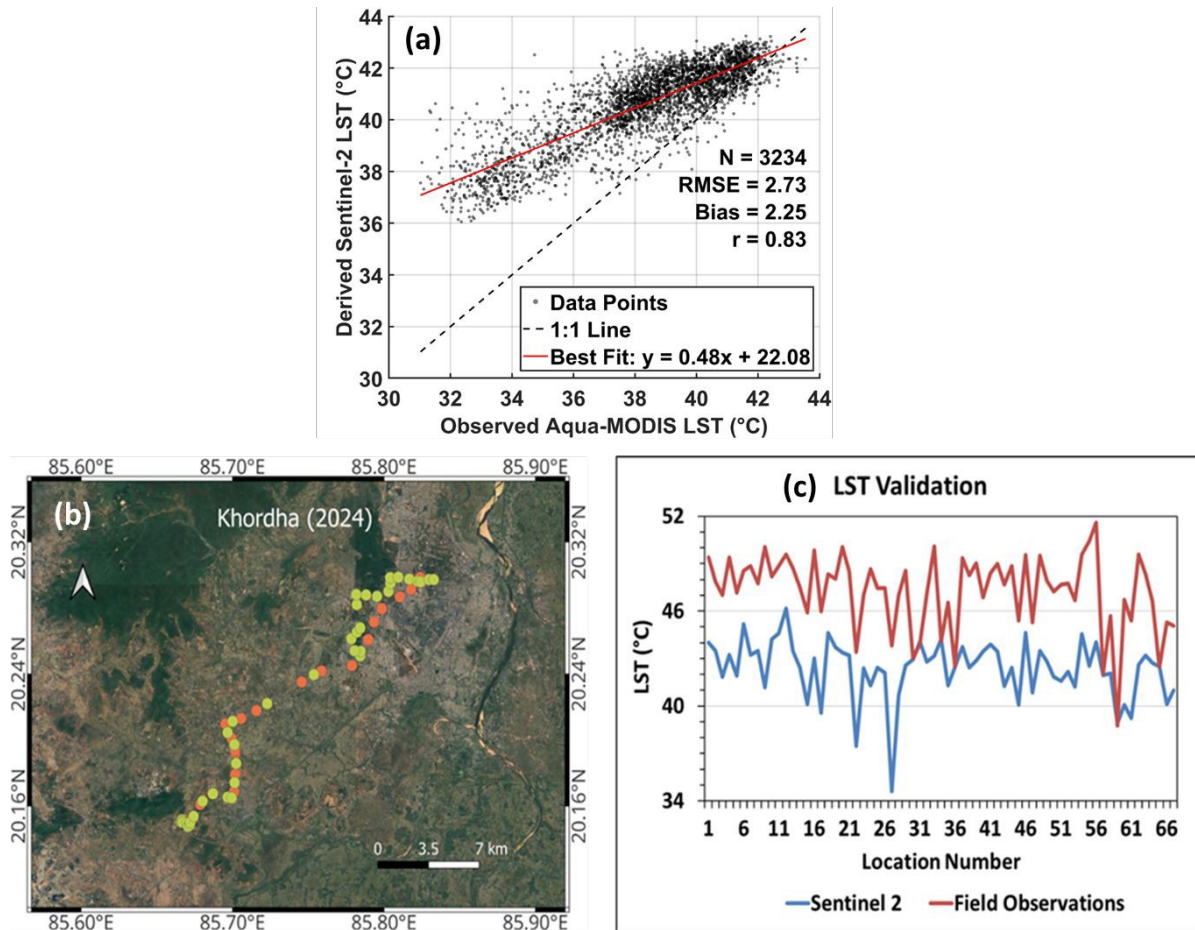


237 **Fig. 3** Mean and standard deviation (SD) of LST, along with the trendline and Sen's slope statistics for the 30 districts
238 of Odisha during the pre-monsoon season of 2017 to 2023.

239

240 To validate the downscaled LST, a methodological comparison between the derived Sentinel-2 LST and the Aqua-
241 MODIS LST was first conducted (Figure 4a). This showed a strong positive Pearson's correlation coefficient ($r =$
242 0.83), and a low root mean square error (RMSE) of 2.73°C, confirming that the spatial patterns captured by Sentinel-
243 2 LST were reasonably consistent with the MODIS benchmark considering the nature of study. An earlier
244 intercomparison by Andriambololonaharisoamalala et al. (2025)⁶⁷ also yielded similar correlation ($r = 0.85$) and
245 RMSE of 2.7 °C for a similar cross-platform LST downscaling framework. The small positive bias of 2.25 °C was
246 likely due to the fact that Sentinel-2, even when aggregated, preserves thermal signatures from high thermal intensity
247 surfaces (such as industrial roofs or bare rock) that may be more heavily smoothed by the coarser resolution MODIS
248 sensor. The overall clustering of data points demonstrated that the downscaling methodology effectively preserved
249 the broad spatial thermal patterns and baseline radiometric characteristics of the original MODIS data and translated
250 it into the derived high-resolution LST. Field validation of the derived high-resolution LST was carried out by inter-
251 comparison with in-situ observations for the Khordha district during the pre-monsoon season of 2024 (Figure 4b-c).
252 Three major land cover types were considered for validation, namely, barren land, vegetation, and built-up areas,
253 involving 68 satellite and in situ collocated points. A moderate correlation of 0.54 was observed between the two
254 datasets.⁶⁸ Additionally, the downscaled LSTs were found to be underestimated, as indicated by a bias of -4.9 °C, and
255 RMSE of 5.3 °C. The observed discrepancy in error margins, i.e., a lower error during the satellite-to-satellite
256 methodological validation compared to the satellite-to-ground field validation, could be primarily attributed to spatial
257 scale mismatch and land surface heterogeneity. The methodological validation compared two satellite-derived
258 radiometric products that inherently averaged thermal signals over varying pixel areas, leading to stronger statistical
259 agreement. Conversely, field observations represented highly localized point measurements that captured singular
260 LSTs, which a satellite pixel inherently smoothed out.

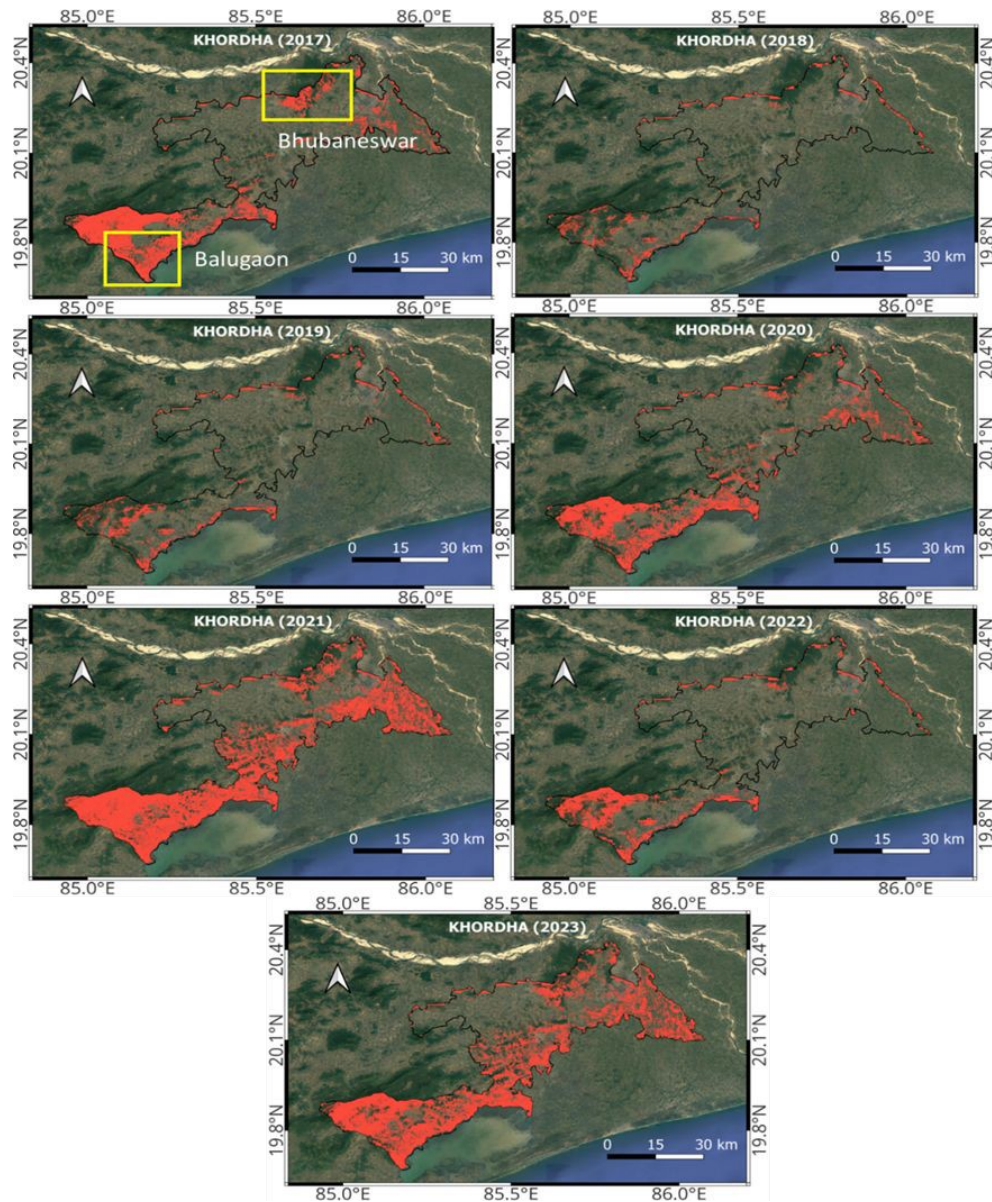




262
263 **Fig. 4** (a) Methodological comparison between derived Sentinel-2 LST and observed Aqua-MODIS LST, with
264 statistical and error metrics given on the plot. (b) Locations of in situ observation points in Khordha district during 2nd
265 March (orange dots) and 11th May (yellow dots) of the 2024 pre-monsoon season. (c) Inter-comparison of the derived
266 Sentinel-2 LST against concurrent field measurements.

267
268 The downscaled LST was then used to identify thermal hotspots by comparing them with the climatology. The
269 hotspots over Khordha district during the study period are presented in Figure 5. The yellow boxes in Figure 5 indicate
270 the urban centers where thermal hotspots were the most prominent. In 2017, the hotspots were mainly distributed in
271 the southern region of the district, while a significant decrease in hotspot area was observed during 2018 and 2019. In
272 2020, the hotspots started to increase again, mainly across the central and southern regions of the study area. However,
273 the highest spread of thermal hotspots was observed in 2021, and followed by 2023, exhibiting significant inter-annual
274 variability.





275
276 **Fig. 5** Distribution of thermal hotspots during the pre-monsoon season of 2017 to 2023 over Khordha district, Odisha.

277
278 Overall, the thermal hotspots over the Khordha region had an increasing trend in the past seven years. Since the overall
279 temperatures are currently on the rise, it is only normal that most regions are experiencing an increase in LST,
280 sometimes even above the 90th percentile threshold. Consequently, thermal hotspots have been identified over several
281 vegetated regions and fallow lands in the study area over the years. An example of such a region is the southwestern
282 part of Khordha district, where LST over a reserved forest was observed to be exceeding the 90th percentile threshold
283 of its climatology. The detailed characterization of Khordha in this section was primarily chosen due to its well-



284 documented status as the most urbanized region in Odisha⁶⁹, serving as a primary indicator for urban thermal stress.
285 However, this phenomenon was not isolated to this single district. Similar extensive thermal hotspot occurrences were
286 observed across various other districts throughout the state, driven by a diverse array of localized mechanisms
287 including industrial expansion, open-cast mining, and severe forest degradation. Crucially, much like the patterns
288 observed in Khordha, these widespread hotspots exhibited significant inter-annual variability across the study period,
289 detailed in the subsequent section.

290

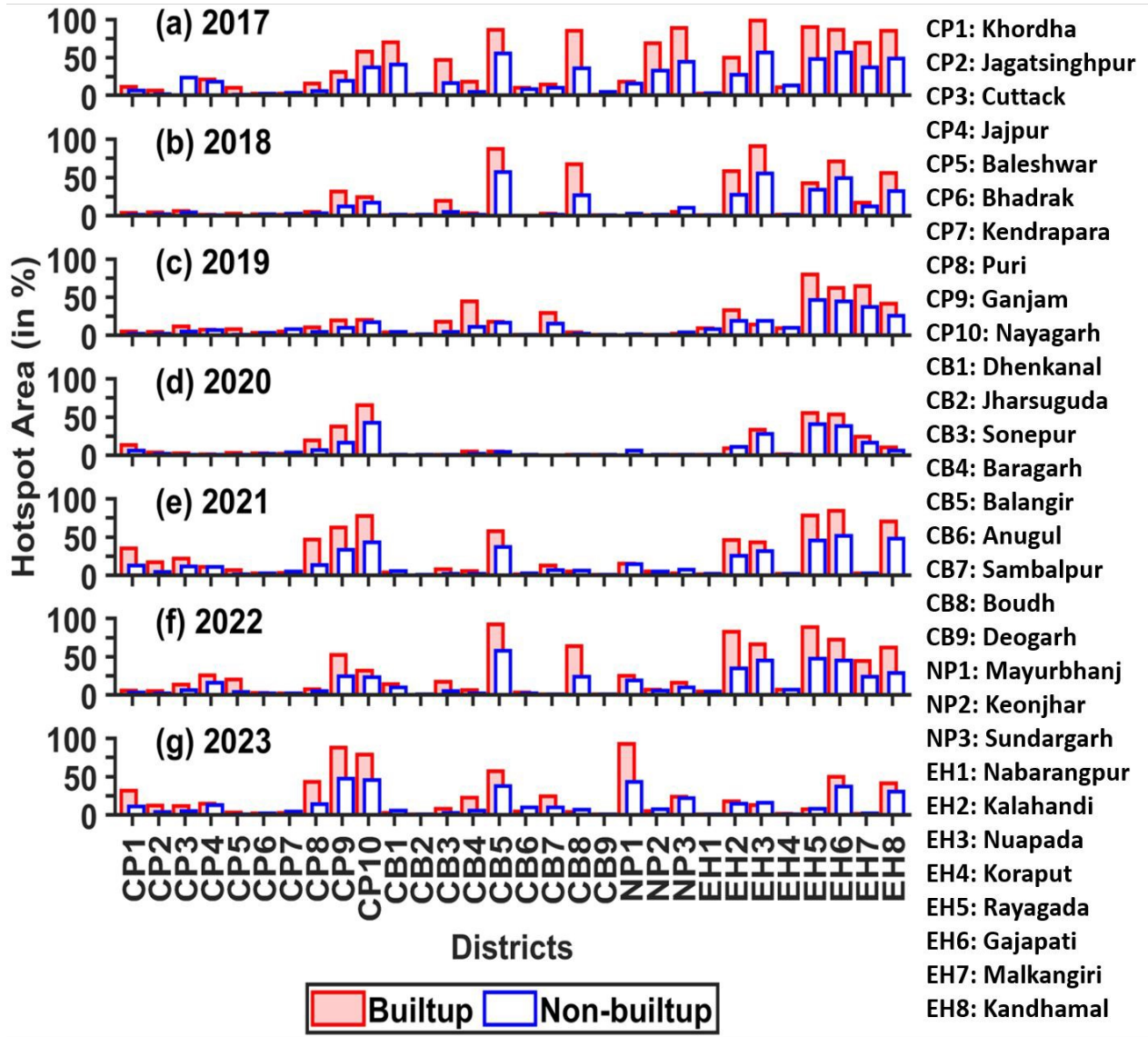
291 **3.2 Impact of Land use land cover on thermal hotspot formation**

292 Sentinel-2 LULC was used to assess the influence of land cover on the distribution of hotspots over the study area.
293 The hotspots were broadly segregated into two categories, over built-up and non-builtup land covers. The percentage
294 of hotspots over each of these two land covers is presented as grouped bar plots in Figure 6. The y-axis represents the
295 percentage of hotspot areas, while the x-axis corresponds to the districts numbered similar to Table 1. Built-up areas
296 (red bars) comprise a significantly higher proportion of hotspots compared to non-builtup areas (blue bars), indicating
297 the impact of urbanization on increasing thermal hotspots in recent years. It was observed that Khordha, Cuttack,
298 Sambalpur, Sundargarh, Angul, and Jharsuguda, all highly urbanized and industrial districts, exhibited the highest
299 percentage of hotspot areas over built-up land covers. The high thermal capacity of these built-up land covers makes
300 these regions more prone to higher daytime temperatures and higher occurrences of thermal hotspots, as similarly
301 observed in previous studies.^{70,71} In contrast, hotspot areas in non-builtup land cover were notably higher in western
302 and interior regions of Odisha in CB and EH zones, such as Bargarh, Balangir, Kalahandi and Nuapada. These districts,
303 although previously agrarian, have recently experienced a prevalence of barren lands, fallow agricultural land, and
304 areas impacted by deforestation. Such a change in the natural land covers diminishes the natural cooling effect and
305 leads to elevated LSTs, which may have led to the formation of thermal hotspots over the non-builtup regions.⁷²
306 However, Sundargarh district is unique in this sense, showing high hotspot areas in both built-up and non-builtup
307 regions. This indicated a mix of urban and natural surface heating effects in the district. Overall, the results highlighted
308 a clear pattern where urban centers in the NP and CP districts experienced a higher proportion of hotspots in built-up
309 areas, while western and interior districts exhibited more heat concentration in non-builtup land covers.

310

311





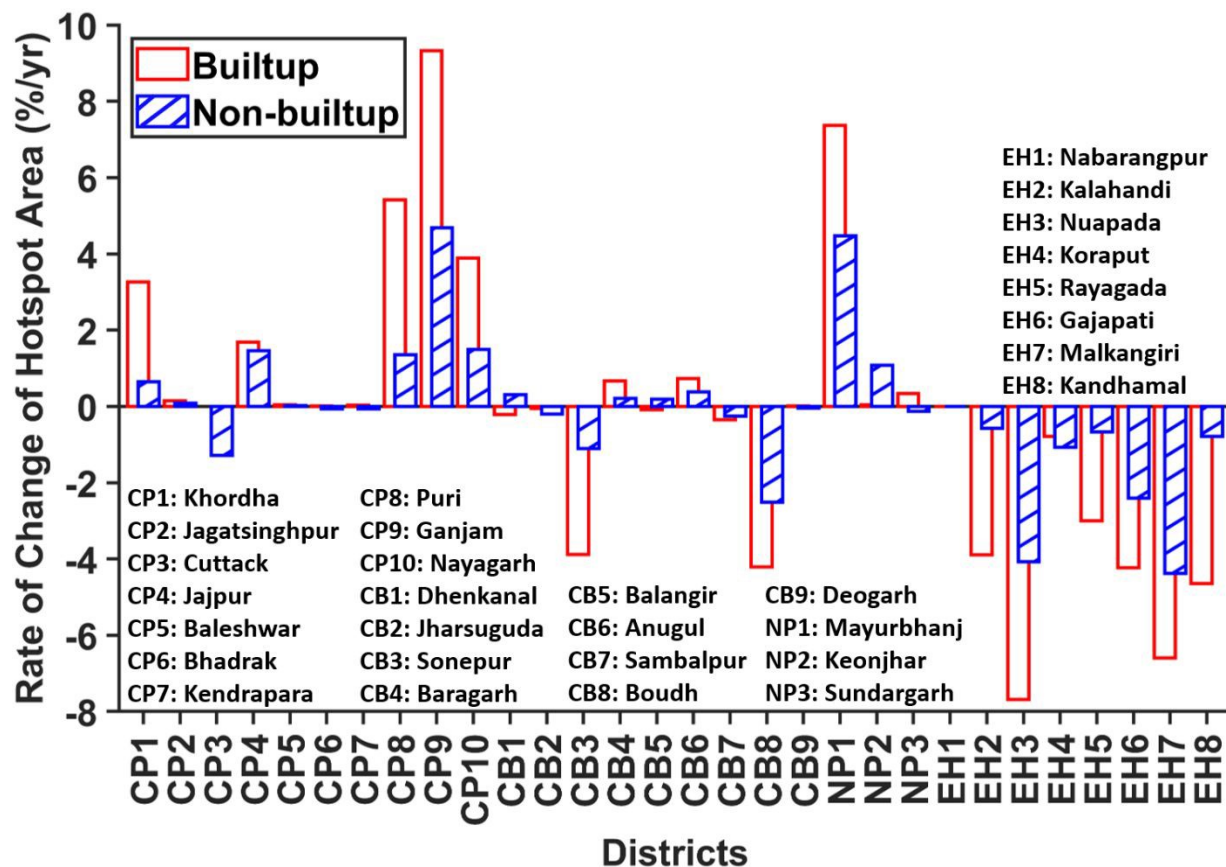
Open Access Article. Published on 28 May 2026. Downloaded on 5/30/2026 1:10:57 PM.
 This article is licensed under a Creative Commons Attribution-NonCommercial 3.0 Unported Licence.

312
 313 **Fig. 6** Percentage of hotspot areas in built-up and non-builtup land cover across the 30 districts of Odisha. Panels a–g
 314 represent the years from 2017 to 2023, respectively.
 315
 316 Changes in the percentage cover of hotspots over built-up and non-builtup regions were estimated using a trend
 317 analysis. The rates of change of hotspot area (% per year) over built-up and non-builtup land covers across Odisha are
 318 shown in Figure 7. From the figure, it is evident that certain coastal districts, such as Ganjam, Kendrapara, and
 319 Khordha, along with Balangir and Mayurbhanj, exhibited a significant increasing trend in hotspot areas over the built-
 320 up regions. Among these, Ganjam district showed the highest rate of change in hotspots over both built-up and non-
 321 builtup land covers. Such trends are indicative of rapid urbanization and infrastructure expansion in these districts,

Environmental Science: Advances Accepted Manuscript

322 leading to intensified land surface heating.⁷³ Similarly, districts like Gajapati, Nabarangpur, and Sonepur in the eastern
 323 hill regions also showed a significant rise in hotspot areas in both built-up and non-builtup regions. Conversely, several
 324 districts in the coastal and northern Odisha, including Cuttack, Balangir, Sundargarh, and Sambalpur, exhibited a
 325 decreasing trend in hotspot areas over built-up land, potentially reflecting increased vegetation or climate-related
 326 variations reducing heat accumulation. Interestingly, districts in the EH zone showed a decreasing percentage of
 327 hotspots over both builtup and non-builtup land covers. These districts are all situated at higher elevations (more than
 328 200 m above mean sea level), have low population densities, and are among the major vegetated regions of the state.
 329 Some districts, such as Jagatsinghpur and Dhenkanal, showed relatively low trends, showing minimal changes in
 330 hotspot areas over time.

331



332

333 Fig. 7 Percentage change per year in hotspot area over builtup and non-builtup land covers across the 30 districts of
 334 Odisha.

335

336 **3.3 Persistent thermal hotspot occurrences over Odisha**



337 The spatial distribution of PTH across Odisha revealed stark regional contrasts intimately tied to the state's four
338 primary geographic typologies, driven by distinct land surface mechanisms. Table 2 presents a district-wise account
339 of the total area and percentage of that area covered by PTH for the 30 districts of Odisha. Figure 8 depicts the spatial
340 distribution of these PTH occurrences for the CP, CB, NP, and EH districts, respectively. In the CP districts, the region
341 generally experienced low-to-moderate thermal vulnerability due to their coastal climate and moist deltaic soils.
342 Northern districts like Baleswar (3.42%) and Bhadrak (4.22%) were observed to have minimal PTH coverage.
343 However, severe exceptions emerged in Nayagarh (76.05%) and Ganjam (40.70%). In these areas, extreme heat
344 heavily aligned with topographical heat trapping, exposed sandy shorelines, and the receding margins of shallow water
345 bodies like Chilika Lake. Furthermore, dynamic urban land covers in rapidly urbanizing coastal cities experienced
346 intense episodes of heat. However, the frequent alteration of land covers in these expanding urban centers often
347 disrupted the temporal continuity needed to classify them as static, long-term PTH. Moving inland to the CB districts,
348 the thermal landscape transitioned into a more fragmented but intensely concentrated pattern. While the region
349 contained highly stable thermal environments in districts like Deogarh (1.57%) and Angul (3.01%), Balangir (75.02%)
350 stood out as a massive and contiguous thermal anomaly. Heat clusters in this typology were heavily sustained by
351 established open mines and heavily modified industrial corridors that absorbed maximum solar radiation.
352 Additionally, major river networks like the Mahanadi and Brahmani actively contributed to localized thermal stress,
353 as seasonally decreasing water level exposed expansive, rapidly heating dry river beds. In the NP districts, a
354 comparatively more variable susceptibility to persistent heating was observed. Extensive open mines and localized
355 industrial clearings contributed to focused, severe heat clusters across this elevated terrain in the region. Finally, the
356 EH districts demonstrated the most extensive and contiguous thermal vulnerability in the entire state. A record-high
357 thermal stress engulfed Rayagada (92.09%) and Gajapati (86.16%), alongside a severe continuous belt covering
358 Nuapada (66.14%), Kandhamal (62.56%), and Kalahandi (60.87%). This widespread, persistent heat could be
359 primarily driven by the degradation of natural forests, extensive shifting cultivation, and the rapid pre-monsoon
360 heating of barren rocky terrains. Only a few districts like Nabarangpur (3.66%) and Koraput (4.07%) maintained
361 exceptionally low coverages, which could be attributed to surviving intact canopies and localized moisture retention.
362



363

Table 2 Areal coverage of PTH over the 30 districts of Odisha

Sl. No.	Name	Area (km ²)	% Area of PTH	Sl. No.	Name	Area (km ²)	% Area of PTH
CP1	Khordha	2733.19	8.17	EH1	Nabarangpur	5260.06	3.66
CP2	Jagatsinghpur	1705.57	5.37	EH2	Kalahandi	7927.29	60.87
CP3	Cuttack	3897.49	16.93	EH3	Nuapada	3889.42	66.14
CP4	Jajpur	2880.89	18.62	EH4	Koraput	8624.38	4.07
CP5	Baleswar	3834.45	3.42	EH5	Rayagada	7397.67	92.09
CP6	Bhadrak	2510.02	4.22	EH6	Gajapati	4052.38	86.16
CP7	Kendrapara	2468.57	7.16	EH7	Malkangiri	5762.22	36.36
CP8	Puri	3596.38	20.91	EH8	Kandhamal	8057.16	62.56
CP9	Ganjam	8533.47	40.70	NP1	Mayurbhanj	10444.80	27.93
CP10	Nayagarh	3892.92	76.05	NP2	Keonjhar	8307.68	5.61
CB1	Dhenkanal	4520.54	6.42	NP3	Sundargarh	9716.67	18.57
CB2	Jharsuguda	2105.96	2.64				
CB3	Sonepur	2376.07	9.68		Prefix	Geographical Region	
CB4	Baragarh	5761.67	8.57		CP:	Coastal Plains	
CB5	Balangir	6642.63	75.02		CB:	Central River Basins	
CB6	Angul	6379.63	3.01		EH:	Eastern Hills	
CB7	Sambalpur	6720.26	14.24		NP:	Northern Plateau	
CB8	Boudh	3069.57	15.97				
CB9	Deogarh	2796.53	1.57				

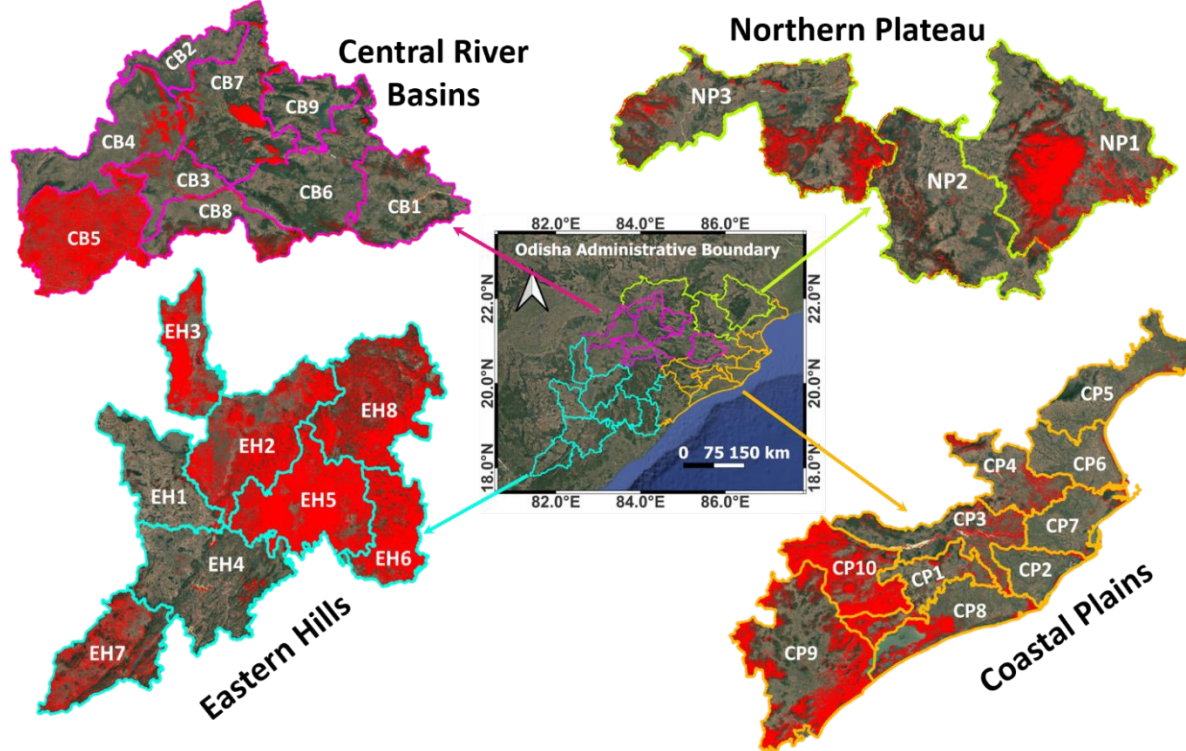
Districts in each zone are sorted based on their population density

364

365 Despite belonging to varying geographic typologies, the districts recording the most extreme thermal vulnerability,
 366 namely Kalahandi, Nuapada, Rayagada, Gajapati and Kandhamal in the EH region, Balangir in the CB region, and
 367 Nayagarh in the CP region, shared a critical underlying mechanism. Their exceptionally high PTH occurrences were
 368 uniformly driven by the sheer dominance of structurally static, high-thermal-inertia landscapes that lacked evaporative
 369 cooling during the pre-monsoon season. Because the analytical methodology required a region to consistently exceed
 370 a high-temperature threshold to be classified as a PTH, these intense thermal signatures only formed over landscapes
 371 devoid of rapid land-cover changes. Whether it was the degraded hillslopes and shifting agricultural tracts of the EH
 372 districts, or the topographically enclosed, barren terrains and flood plains of Balangir and Nayagarh, these
 373 environments all suffered from a profound absence of substantial vegetative canopy and soil moisture. Consequently,



374 without plants or surface water to facilitate evaporative cooling, these bare, exposed surfaces absorbed maximum solar
 375 radiation and sustained extreme temperatures to be classified as PTH consistently throughout the study period.
 376



377
 378 **Fig. 8** PTH occurrences (in red) over the districts of Odisha.
 379

380 It would be prudent to note that since these hotspots represented chronic, structurally unchanging heat reservoirs, they
 381 could easily subject local communities to prolonged heat stress. To mitigate the PTH occurrences across these districts,
 382 a multi-pronged approach focusing on urban cooling and ecological restoration may be essential. In industrial and
 383 urban hubs like Sundergarh, Khordha, Jajpur, and Jagatsinghpur districts, mitigation should prioritize cool
 384 infrastructure by implementing reflective roofing, permeable pavements, and vertical gardens to counteract the high
 385 thermal inertia of concrete.⁷⁴ Expanding urban forestry and creating green corridors would provide critical shading
 386 and evaporative cooling, effectively mimicking the naturally vegetated region. For coastal districts like Baleswar,
 387 Bhadrak, and Kendrapara, protecting and expanding coastal mangrove ecosystems would prove to be vital. These
 388 dense mangrove canopies would offer superior thermal regulation and moisture retention compared to exposed sandy
 389 coastlines.⁷⁵ In the vast agricultural and riverine belts of Cuttack, Puri, Ganjam, and Nayagarh, the focus should shift



390 toward sustainable land management and water conservation. For hotspots tracing the dry beds of the Mahanadi,
391 Brahmani, and Baitarani rivers, integrated watershed management and the restoration of riparian vegetation would
392 significantly enhance localized cooling. Furthermore, protecting the forested highlands of the Eastern Ghats would be
393 equally crucial, as these natural thermal buffers would provide the regional moisture and shade necessary to stabilize
394 temperatures in the adjacent heating plains.

395

396 **3.4 Population Exposure to Thermal Hotspots**

397 While the identification of PTH delineated the spatial distribution of long-term environmental heat, analyzing
398 population exposure provided a crucial anthropogenic dimension to understanding this vulnerability. Analysis
399 revealed clear inter-annual variability and regional heterogeneity in how this thermal stress impacted local
400 communities. In terms of absolute numbers, districts like Ganjam, Sundargarh, Khordha, and Cuttack experienced the
401 highest population exposure statewide. This vulnerability was primarily because these districts encompassed Odisha's
402 major urban, commercial, and industrial centers. The high exposure in CP districts, like Khordha, Cuttack, and
403 Ganjam, was driven by their status as dense metropolitan hubs characterized by extensive built environments and high
404 population densities. Similarly, the elevated exposure in Sundargarh, situated in the NP region, was heavily influenced
405 by anthropogenic heat generation stemming from large-scale industrial activities. Figure 9 depicts the percentage of
406 the total district population exposed to these hotspots. This approach provided a normalized intercomparable indicator
407 of population exposure in the 30 districts of Odisha. The highest proportional exposures were consistently observed
408 in the EH and select districts of the CP regions. Notably, Rayagada and Nayagarh demonstrated persistent
409 vulnerability, recording significant exposure levels almost every year throughout the study period. Conversely, sub-
410 regions within the NP and the majority of the CB districts displayed generally lower and less consistent exposure
411 percentages. This trend suggested that these areas either possessed localized microclimates less susceptible to forming
412 widespread thermal hotspots, or their populations were geographically distributed outside the primary heat zones. A
413 closer temporal analysis of the seven-year period revealed distinct climatological and anthropogenic patterns. The
414 years 2017 (Figure 9a) and 2022 (Figure 9f) stood out in the data, exhibiting high and widespread percentage exposure
415 across multiple sub-regions, indicating periods of elevated, state-wide thermal stress. In contrast, the year 2020 (Figure
416 9d) exhibited the lowest exposure to thermal hotspots across the entire dataset, with the metrics for almost all districts
417 dropping notably. This reduction in exposed populations could directly be attributed to the pandemic-induced



lockdowns, reducing major anthropogenic disruptions (industrial operations, vehicular traffic, and overall urban activity), leading to lower surface temperatures.⁷⁶

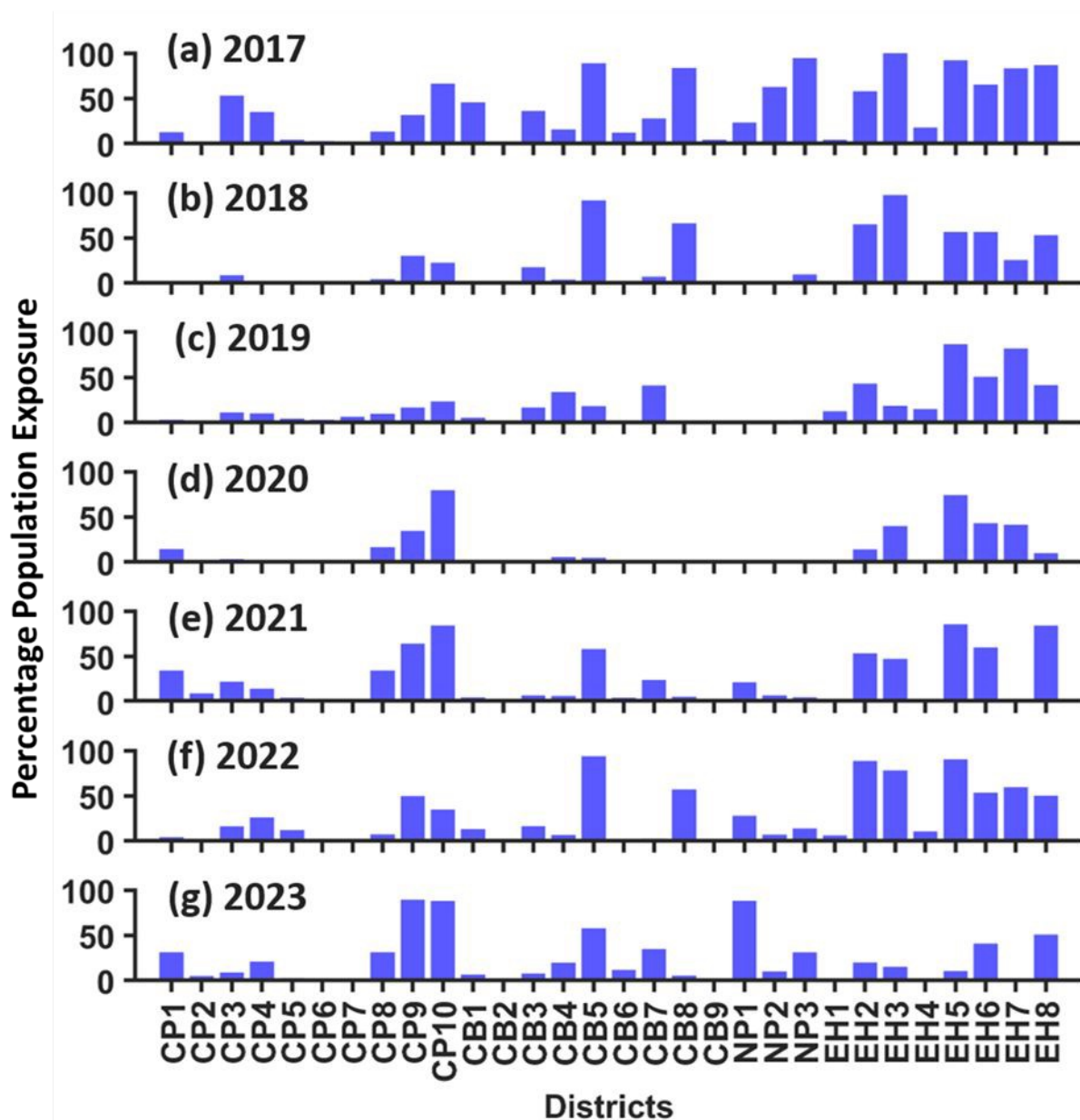


Fig. 9 Yearly percentage population exposure in the 30 districts of Odisha from 2017 to 2023.

420

421

422

Overall, the study's findings revealed that the proliferation of thermal hotspots in the built-up areas of Odisha's

urbanizing districts, such as Khordha and Ganjam, was attributable to the transformation of natural, permeable

surfaces into impervious ones like asphalt and concrete. These artificial materials possess higher thermal capacity,

causing them to absorb more solar radiation and retain heat for longer periods. The observed increasing trend of



427 hotspots in these specific districts directly reflected their ongoing, rapid infrastructure development and population
428 growth. A particularly crucial finding was the geographical diversity in hotspot distribution, where the hotspots of
429 western and interior districts like Bargarh and Kalahandi were governed by the thermal conditions in non-built-up
430 areas. This challenged the simplistic view that only urban areas were prone to extreme heat. The prevalence of hotspots
431 in these agrarian and semi-arid regions was driven by land degradation factors such as deforestation, barren lands, and
432 fallow agricultural fields during the dry pre-monsoon season. This indicates that land management practices, not just
433 urbanization, are critical drivers of regional thermal stress. The unique case of Sundargarh, which exhibited significant
434 hotspots in both built-up and non-built-up areas, exemplified a complex scenario where industrial heating compounds
435 the effects of degraded natural landscapes. Several studies have linked an increase in vector-borne diseases and human
436 health issues with rising temperatures and other climate extremes in Odisha.^{18,20-22,37} The projected increase in
437 population density in the urban-industrial regions will also enhance the exposure of its inhabitants to extreme heat. In
438 such a situation, an increase in the frequency and coverage of urban thermal hotspots at the current rate would
439 exacerbate this situation and pose a severe risk to sustainable and comfortable living, especially in the rapidly
440 urbanizing regions of developing countries like India.⁷⁷ However, the significant drop in population exposure observed
441 during the 2020 period suggests a viable countermeasure, demonstrating that implementing strategic, temporary
442 reductions in urban and industrial activities, during peak thermal events could possibly serve as an effective,
443 immediate policy tool to mitigate impacts of heat stress on vulnerable populations.

444

445 **4. Conclusion**

446 This study provides a comprehensive analysis of thermal hotspots across 30 districts of Odisha, India, focusing on the
447 differences between built-up and non-builtup land covers during pre-monsoon seasons of 2017 to 2023. The findings
448 revealed a significant increase in thermal hotspots in highly urbanized districts such as Khordha, Ganjam, Sundargarh,
449 and Sambalpur, where rapid urban expansion and impervious surface growth contributed to rising temperatures.
450 Conversely, interior districts like Bargarh, Balangir, and Kalahandi exhibited more pronounced hotspot areas in non-
451 builtup regions, primarily due to the conversion of natural vegetated land covers into fallow agricultural and barren
452 lands. It was also observed that the abundance of paved surfaces and densely packed infrastructure led to an increase
453 in persistent hotspots, whereas urban forests and vegetated regions helped alleviate the heat stress. Consequently,
454 significant population exposure to thermal stress could be avoided with timely knowledge of PTHs. This study hence



455 proposes targeted mitigation efforts in regions under extreme heat stress and thermal hotspot occurrences. Increasing
456 urban greenery, implementing heat-resilient infrastructure, and promoting sustainable land-use policies that balance
457 development with environmental conservation can help reduce surface heating, minimize health risks, and lead society
458 towards a more harmonious living with nature.

459

460 **Author Contributions**

461 **DM** – Conceptualization, Data curation, Formal analysis, Investigation, Methodology, Software, Validation,
462 Visualization, Writing – original draft; **DS** – Conceptualization, Investigation, Methodology, Resources, Supervision,
463 Writing – original draft.

464

465 **Conflicts of Interest**

466 The authors declare that they do not have any known competing interests whatsoever associated with this study.

467

468 **Funding Statement**

469 This research received no specific funding.

470

471 **Data Availability**

472 All satellite datasets used in this study are available on public domains. Field observations and codes can be made
473 available on request to the corresponding author.

474

475 **Acknowledgements**

476 The authors acknowledge IIT Bhubaneswar for providing the infrastructure to carry out this study the various agencies
477 for providing the satellite data used in this work. The authors are also grateful to the anonymous reviewers whose
478 comments and suggestions have contributed to improve the manuscript contents immensely.

479



480 **References**

- 481 1. Lambin EF, Geist HJ, Lepers E. Dynamics of land-use and land-cover change in tropical regions. *Annu Rev*
482 *Environ Resour* [Internet]. 2003;28(1):205–41. Available from:
483 <http://dx.doi.org/10.1146/annurev.energy.28.050302.105459>
- 484 2. Swain D, Roberts GJ, Dash J, Lekshmi K, Vinoj V, Tripathy S. Impact of rapid urbanization on the city of
485 Bhubaneswar, India. *Proc Nat Acad Sci India Sect A* [Internet]. 2017;87(4):845–53. Available from:
486 <http://dx.doi.org/10.1007/s40010-017-0453-7>
- 487 3. Roy PS, Ramachandran RM, Paul O, Thakur PK, Ravan S, Behera MD, et al. Anthropogenic land use and land
488 cover changes—A review on its environmental consequences and climate change. *J Ind Soc Remote Sens*
489 [Internet]. 2022;50(8):1615–40. Available from: <http://dx.doi.org/10.1007/s12524-022-01569-w>
- 490 4. Santamouris M. Regulating the damaged thermostat of the cities—Status, impacts and mitigation challenges.
491 *Energy Build* [Internet]. 2015;91:43–56. Available from: <http://dx.doi.org/10.1016/j.enbuild.2015.01.027>
- 492 5. Golden JS. The built environment induced urban heat island effect in rapidly urbanizing arid regions—a
493 sustainable urban engineering complexity. *Environ Sci*. 2004;1(4):321–49.
- 494 6. Obiakor MO, Ezeonyejaku CD, Mogbo TC. Effects of vegetated and synthetic (impervious) surfaces on the
495 microclimate of urban area. *J Applied Sci Environ Management*. 2012;16(1):85–94.
- 496 7. Devanathan P, Devanathan K. Heat island effects. In: Sabnis GM, editor. *Green Building with Concrete:*
497 *Sustainable Design Construction* [Internet]. London, England: Taylor & Francis; 2011. p. 175–226. Available
498 from: <https://bayanbox.ir/view/3322753378973510188/1439812969-a.pdf>
- 499 8. Hua AK, Ping OW. The influence of land-use/land-cover changes on land surface temperature: a case study of
500 Kuala Lumpur metropolitan city. *Eur J Remote Sens* [Internet]. 2018;51(1):1049–69. Available from:
501 <http://dx.doi.org/10.1080/22797254.2018.1542976>
- 502 9. Kafy A-. A, Rahman MS, Faisal A-A-, Hasan MM, Islam M. Modelling future land use land cover changes and
503 their impacts on land surface temperatures in Rajshahi, Bangladesh. *Remote Sens Appl Soc Environ* [Internet].
504 2020;18(100314):100314. Available from: <http://dx.doi.org/10.1016/j.rsase.2020.100314>
- 505 10. Ramzan M, Saqib ZA, Hussain E, Khan JA, Nazir A, Dasti MYS, et al. Remote sensing-based prediction of
506 temporal changes in land surface temperature and land use-land cover (LULC) in urban environments. *Land*
507 (Basel) [Internet]. 2022;11(9):1610. Available from: <http://dx.doi.org/10.3390/land11091610>



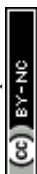
- 508 11. Yao R, Wang L, Huang X, Gong W, Xia X. Greening in rural areas increases the surface urban heat island
509 intensity. *Geophys Res Lett* [Internet]. 2019;46(4):2204–12. Available from:
510 <http://dx.doi.org/10.1029/2018gl081816>
- 511 12. Gohain KJ, Mohammad P, Goswami A. Assessing the impact of land use land cover changes on land surface
512 temperature over Pune city, India. *Quat Int* [Internet]. 2021;575–576:259–69. Available from:
513 <http://dx.doi.org/10.1016/j.quaint.2020.04.052>
- 514 13. Srikanth K, Swain D. Urbanization and Land surface temperature changes over Hyderabad, a semi-arid mega
515 city in India. *Remote Sens Appl Soc Environ* [Internet]. 2022;28(100858):100858. Available from:
516 <http://dx.doi.org/10.1016/j.rsase.2022.100858>
- 517 14. Weng Q. Thermal infrared remote sensing for urban climate and environmental studies: Methods, applications,
518 and trends. *ISPRS J Photogramm Remote Sens* [Internet]. 2009;64(4):335–44. Available from:
519 <http://dx.doi.org/10.1016/j.isprsjprs.2009.03.007>
- 520 15. Kestens Y, Brand A, Fournier M, Goudreau S, Kosatsky T, Maloley M, et al. Modelling the variation of land
521 surface temperature as determinant of risk of heat-related health events. *Int J Health Geogr* [Internet]. 2011 [cited
522 2025 Nov 5];10(1):7. Available from: <http://www.ij-healthgeographics.com/content/10/1/7>
- 523 16. White-Newsome JL, Brines SJ, Brown DG, Dvonch JT, Gronlund CJ, Zhang K, et al. Validating satellite-derived
524 land surface temperature with in situ measurements: a public health perspective. *Environ Health Perspect*
525 [Internet]. 2013;121(8):925–31. Available from: <http://dx.doi.org/10.1289/ehp.1206176>
- 526 17. Abdel-Ghany AM, Al-Helal IM, Shady MR. Human thermal comfort and heat stress in an outdoor urban arid
527 environment: A case study. *Adv Meteorol* [Internet]. 2013;2013:1–7. Available from:
528 <http://dx.doi.org/10.1155/2013/693541>
- 529 18. Mohammadi A, Mashhoodi B, Shamsoddini A, Pishgar E, Bergquist R. Land surface temperature predicts
530 mortality due to chronic obstructive pulmonary disease: a study based on climate variables and impact machine
531 learning. *Geospat Health* [Internet]. 2025;20(1). Available from: <http://dx.doi.org/10.4081/gh.2025.1319>
- 532 19. Wang P, Yang Y, Li H, Chen L, Dang R, Xue D, et al. North China Plain as a hot spot of ozone pollution
533 exacerbated by extreme high temperatures. *Atmos Chem Phys* [Internet]. 2022;22(7):4705–19. Available from:
534 <http://dx.doi.org/10.5194/acp-22-4705-2022>



- 535 20. Savioli G, Zanza C, Longhitano Y, Nardone A, Varesi A, Ceresa IF, et al. Heat-related illness in emergency and
536 critical care: Recommendations for recognition and management with medico-legal considerations.
537 Biomedicines [Internet]. 2022;10(10):2542. Available from: <http://dx.doi.org/10.3390/biomedicines10102542>
- 538 21. O'Connor FG. Heat-related illnesses. *Ann Intern Med* [Internet]. 2025;178(7):ITC97–112. Available from:
539 <http://dx.doi.org/10.7326/ANNALS-25-01958>
- 540 22. Kenny GP, Yardley J, Brown C, Sigal RJ, Jay O. Heat stress in older individuals and patients with common
541 chronic diseases. *Canadian Med Assoc J* [Internet]. 2010;182(10):1053–60. Available from:
542 <http://dx.doi.org/10.1503/cmaj.081050>
- 543 23. Estoque RC, Murayama Y, Myint SW. Effects of landscape composition and pattern on land surface temperature:
544 An urban heat island study in the megacities of Southeast Asia. *Sci Total Environ* [Internet]. 2017;577:349–59.
545 Available from: <http://dx.doi.org/10.1016/j.scitotenv.2016.10.195>
- 546 24. Caseiro A, Rucker G, Tiemann J, Leimbach D, Lorenz E, Frauenberger O, et al. Persistent Hot Spot detection
547 and characterisation using SLSTR. *Remote Sens (Basel)* [Internet]. 2018;10(7):1118. Available from:
548 <http://dx.doi.org/10.3390/rs10071118>
- 549 25. Mavrakou T, Polydoros A, Cartalis C, Santamouris M. Recognition of thermal hot and cold spots in urban areas
550 in support of mitigation plans to counteract overheating: Application for Athens. *Climate* [Internet].
551 2018;6(1):16. Available from: <http://dx.doi.org/10.3390/cli6010016>
- 552 26. Zhang P, Yuan C, Sun Q, Liu A, You S, Li X, et al. Satellite-based detection and characterization of industrial
553 heat sources in China. *Environ Sci Technol* [Internet]. 2019;53(18):11031–42. Available from:
554 <http://dx.doi.org/10.1021/acs.est.9b02643>
- 555 27. Mullerova D, Williams M. Satellite monitoring of thermal performance in smart urban designs. *Remote Sens*
556 (Basel) [Internet]. 2019;11(19):2244. Available from: <http://dx.doi.org/10.3390/rs11192244>
- 557 28. Wang Z, Sun X, Wang H. Threshold-driven modeling of urban heat exposure under impervious surface
558 expansion: a decadal remote sensing assessment of Shanghai. *Stoch Environ Res Risk Assess* [Internet].
559 2026;40(1). Available from: <http://dx.doi.org/10.1007/s00477-025-03150-6>
- 560 29. Karami P, Mousavi S-M. Spatiotemporal analysis of thermal islands in a semi-arid city: A case study of
561 Kermanshah, Iran using machine learning and remote sensing. *Environ Chall (Amst)* [Internet].
562 2025;20(101174):101174. Available from: <http://dx.doi.org/10.1016/j.envc.2025.101174>



- 563 30. Sola-Caraballo J, Serrano-Jiménez A, Rivera-Gomez C, Galan-Marin C. Multi-criteria assessment of urban
564 thermal hotspots: A GIS-based remote sensing approach in a Mediterranean climate city. *Remote Sens (Basel)*
565 [Internet]. 2025;17(2):231. Available from: <http://dx.doi.org/10.3390/rs17020231>
- 566 31. Kumari S, Singh R, Singh VB, Chauhan V. A multivariate geostatistical framework to assess the spatio-temporal
567 dynamics of coupled urban–thermal–ecological interactions in the western Himalaya foothills. *Geosystems and*
568 *Geoenvironment* [Internet]. 2026;5(2):100497. Available from: <http://dx.doi.org/10.1016/j.geogeo.2026.100497>
- 569 32. Maroofiazar R, Reveshti AM. Integrating Remote Sensing and Machine Learning for Enhanced Surface Urban
570 Heat Island Analysis and Its Impact on. *Building Energy Demand Energy Science & Engineering*. 2026;
- 571 33. Eingrüber N, Burdová N, Dluhoř V, Domm A, Bongartz M, Nehren U. Hotspots in urban areas: A novel approach
572 to assess the heat mitigation potential of nature-based solutions using microclimate modelling. *Urban Clim*
573 [Internet]. 2026;65(102814):102814. Available from: <http://dx.doi.org/10.1016/j.uclim.2026.102814>
- 574 34. Moges DM, Mattisson K, Malmqvist E, Olsson P-O. Remote sensing of urban heat dynamics and the cooling
575 effect of urban green spaces in Ethiopian cities. *Environ Chall (Amst)* [Internet]. 2026;23(101462):101462.
576 Available from: <http://dx.doi.org/10.1016/j.envc.2026.101462>
- 577 35. Li Z-L, Tang B-H, Wu H, Ren H, Yan G, Wan Z, et al. Satellite-derived land surface temperature: Current status
578 and perspectives. *Remote Sens Environ* [Internet]. 2013;131:14–37. Available from:
579 <http://dx.doi.org/10.1016/j.rse.2012.12.008>
- 580 36. Agathangelidis I, Cartalis C. Improving the disaggregation of MODIS land surface temperatures in an urban
581 environment: a statistical downscaling approach using high-resolution emissivity. *Int J Remote Sens* [Internet].
582 2019;40(13):5261–86. Available from: <http://dx.doi.org/10.1080/01431161.2019.1579386>
- 583 37. Mao Q, Peng J, Wang Y. Resolution enhancement of remotely sensed land surface temperature: Current status
584 and perspectives. *Remote Sens (Basel)* [Internet]. 2021;13(7):1306. Available from:
585 <http://dx.doi.org/10.3390/rs13071306>
- 586 38. Mukherjee S, Joshi PK, Garg RD. Evaluation of LST downscaling algorithms on seasonal thermal data in humid
587 subtropical regions of India. *Int J Remote Sens* [Internet]. 2015;36(10):2503–23. Available from:
588 <http://dx.doi.org/10.1080/01431161.2015.1041175>



- 589 39. Feng X, Foody G, Aplin P, Gosling SN. Enhancing the spatial resolution of satellite-derived land surface
590 temperature mapping for urban areas. *Sustain Cities Soc* [Internet]. 2015;19:341–8. Available from:
591 <http://dx.doi.org/10.1016/j.scs.2015.04.007>
- 592 40. Agam N, Kustas WP, Anderson MC, Li F, Neale CMU. A vegetation index based technique for spatial
593 sharpening of thermal imagery. *Remote Sens Environ* [Internet]. 2007;107(4):545–58. Available from:
594 <http://dx.doi.org/10.1016/j.rse.2006.10.006>
- 595 41. Chen X-L, Zhao H-M, Li P-X, Yin Z-Y. Remote sensing image-based analysis of the relationship between urban
596 heat island and land use/cover changes. *Remote Sens Environ* [Internet]. 2006;104(2):133–46. Available from:
597 <http://dx.doi.org/10.1016/j.rse.2005.11.016>
- 598 42. Guha S, Govil H. A long-term monthly analytical study on the relationship of LST with normalized difference
599 spectral indices. *Eur J Remote Sens* [Internet]. 2021;54(1):487–512. Available from:
600 <http://dx.doi.org/10.1080/22797254.2021.1965496>
- 601 43. Banerjee B, Pal A, Tiwari AK, Kanchan R. Assessing the land use dynamics and thermal environment using
602 geospatial techniques in the industrial city of Chotanagpur Plateau Region, India. *Environ Monit Assess*
603 [Internet]. 2024;196(7):609. Available from: <http://dx.doi.org/10.1007/s10661-024-12752-6>
- 604 44. Karmakar M, Pradhan MM. Climate change and public health: a study of vector-borne diseases in Odisha, India.
605 *Nat Hazards (Dordr)* [Internet]. 2020;102(2):659–71. Available from: [http://dx.doi.org/10.1007/s11069-019-](http://dx.doi.org/10.1007/s11069-019-03594-4)
606 [03594-4](http://dx.doi.org/10.1007/s11069-019-03594-4)
- 607 45. India Meteorological Department. Climate of Orissa [Internet]. 2002. Available from:
608 <https://imdpune.gov.in/library/public/climate%20of%20orissa.pdf>
- 609 46. Government of India. A-01: Number of villages, towns, households, population and area (India, states/UTs,
610 districts and Sub-districts) [Internet]. Census India. 2011 [cited 2025 Apr 1]. Available from:
611 <https://censusindia.gov.in/census.website/data/census-tables>
- 612 47. Farr TG, Rosen PA, Caro E, Crippen R, Duren R, Hensley S, et al. The Shuttle Radar Topography Mission. *Rev*
613 *Geophys* [Internet]. 2007;45(2). Available from: <http://dx.doi.org/10.1029/2005rg000183>
- 614 48. Safieddine S, Clerbaux C, Muñoz-Sabater J, Thépaut J-N. Local hourly trends in near-surface and land surface
615 temperatures. *Sci Rep* [Internet]. 2025;15(1):29915. Available from: [http://dx.doi.org/10.1038/s41598-025-](http://dx.doi.org/10.1038/s41598-025-15731-0)
616 [15731-0](http://dx.doi.org/10.1038/s41598-025-15731-0)



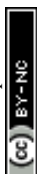
- 617 49. Hesslerová P, Pokorný J, Brom J, Rejšková - Procházková A. Daily dynamics of radiation surface temperature
618 of different land cover types in a temperate cultural landscape: Consequences for the local climate. *Ecol Eng*
619 [Internet]. 2013;54:145–54. Available from: <http://dx.doi.org/10.1016/j.ecoleng.2013.01.036>
- 620 50. Rouse JW, Haas RH, Schell JA, Deering DW, Harlan JC. Monitoring the vernal advancement and retrogradation
621 (greenwave effect) of natural vegetation. NASA/GSFC Type III Final Report. 1974.
- 622 51. Zha Y, Ni SY, Yang S. An Effective Approach to Automatically Extract Urban Land-Use from TM Imagery.
623 *Journal of Remote Sensing*. 2003;7(1):37–40.
- 624 52. Zhao H, Chen X. Use of normalized difference bareness index in quickly mapping bare areas from TM/ETM+.
625 In: *Proceedings 2005 IEEE International Geoscience and Remote Sensing Symposium, 2005 IGARSS '05*. IEEE;
626 2005.
- 627 53. Jin S, Sader SA. Comparison of time series tasseled cap wetness and the normalized difference moisture index
628 in detecting forest disturbances. *Remote Sens Environ* [Internet]. 2005;94(3):364–72. Available from:
629 <http://dx.doi.org/10.1016/j.rse.2004.10.012>
- 630 54. Feng M, Huang C, Channan S, Vermote EF, Masek JG, Townshend JR. Quality assessment of Landsat surface
631 reflectance products using MODIS data. *Comput Geosci* [Internet]. 2012;38(1):9–22. Available from:
632 <http://dx.doi.org/10.1016/j.cageo.2011.04.011>
- 633 55. Liang S, Fang H, Chen M, Shuey CJ, Walthall C, Daughtry C, et al. Validating MODIS land surface reflectance
634 and albedo products: methods and preliminary results. *Remote Sens Environ* [Internet]. 2002;83(1–2):149–62.
635 Available from: [http://dx.doi.org/10.1016/s0034-4257\(02\)00092-5](http://dx.doi.org/10.1016/s0034-4257(02)00092-5)
- 636 56. Misbari S, Zhai W, Doh SI. Comparative analysis between Landsat and MODIS data for urban heat island
637 mapping in Kuala Lumpur. *Constr* [Internet]. 2025;5(2):139–45. Available from:
638 <http://dx.doi.org/10.15282/construction.v5i2.12436>
- 639 57. Zhu S, Zhang H, Liu R, Cao Y, Zhang G. Comparison of sampling designs for estimating deforestation from
640 landsat TM and MODIS imagery: a case study in Mato Grosso, Brazil. *ScientificWorldJournal* [Internet].
641 2014;2014:919456. Available from: <http://dx.doi.org/10.1155/2014/919456>
- 642 58. Lv T, Zhou X, Tao Z, Sun X, Wang J, Li R, et al. Remote sensing-guided spatial sampling strategy over
643 heterogeneous surface ground for validation of vegetation indices products with medium and high spatial



- 644 resolution. Remote Sens (Basel) [Internet]. 2021;13(14):2674. Available from:
645 <http://dx.doi.org/10.3390/rs13142674>
- 646 59. Zhao T, Zhang X, Gao Y, Mi J, Liu W, Wang J, et al. Assessing the accuracy and consistency of six fine-
647 resolution global Land Cover products using a novel stratified random sampling validation dataset. Remote Sens
648 (Basel) [Internet]. 2023;15(9):2285. Available from: <http://dx.doi.org/10.3390/rs15092285>
- 649 60. Massaro E, Schifanella R, Piccardo M, Caporaso L, Taubenböck H, Cescatti A, et al. Spatially-optimized urban
650 greening for reduction of population exposure to land surface temperature extremes. Nat Commun [Internet].
651 2023;14(1):2903. Available from: <http://dx.doi.org/10.1038/s41467-023-38596-1>
- 652 61. Goodchild MF, Anselin L, Deichmann U. A framework for the areal interpolation of socioeconomic data. Environ
653 Plan A [Internet]. 1993;25(3):383–97. Available from: <http://dx.doi.org/10.1068/a250383>
- 654 62. Wu Z, Zhang Y. Water bodies' cooling effects on urban land daytime surface temperature: Ecosystem service
655 reducing heat island effect. Sustainability [Internet]. 2019;11(3):787. Available from:
656 <http://dx.doi.org/10.3390/su11030787>
- 657 63. Jiang Y, Huang J, Shi T, Wang H. Interaction of urban rivers and green space morphology to mitigate the urban
658 heat island effect: Case-based comparative analysis. Int J Environ Res Public Health [Internet].
659 2021;18(21):11404. Available from: <http://dx.doi.org/10.3390/ijerph182111404>
- 660 64. Chen L, Qi Q, Wu H, Feng D, Zhu E. Will the landscape composition and socio-economic development of
661 coastal cities have an impact on the marine cooling effect? Sustain Cities Soc [Internet].
662 2023;89(104328):104328. Available from: <http://dx.doi.org/10.1016/j.scs.2022.104328>
- 663 65. Tarawally M, Xu W, Hou W, Mushore T. Comparative analysis of responses of land surface temperature to long-
664 term land use/cover changes between a coastal and inland city: A case of Freetown and Bo town in Sierra Leone.
665 Remote Sens (Basel) [Internet]. 2018;10(1):112. Available from: <http://dx.doi.org/10.3390/rs10010112>
- 666 66. Jeon G, Park Y, Guldman J-M. Impacts of urban morphology on seasonal land surface temperatures: Comparing
667 grid- and block-based approaches. ISPRS Int J Geoinf [Internet]. 2023;12(12):482. Available from:
668 <http://dx.doi.org/10.3390/ijgi12120482>
- 669 67. Andriambololonaharisoamalala RR, Helmholtz P, Bulatov D, Ivanova I, Song Y, Soon S, et al. Downscaling of
670 urban land surface temperatures using geospatial machine learning with Landsat 8/9 and Sentinel-2 imagery.
671 Remote Sens (Basel) [Internet]. 2025;17(14):2392. Available from: <http://dx.doi.org/10.3390/rs17142392>



- 672 68. A. Ibe A, M. Ogbodo C. Correlation analysis of compaction properties of soil with various soil parameters over
673 Gbaramatu Niger Delta, Nigeria. *Earth Sci Malays* [Internet]. 2023;7(2):96–102. Available from:
674 <http://dx.doi.org/10.26480/esmy.02.2023.96.102>
- 675 69. Census of India. Primary Census Abstract - Data Highlights for Odisha (Series 22) [Internet]. 2011 [cited 2026
676 Mar 21]. Available from:
677 [https://censusindia.gov.in/nada/index.php/catalog/11313/download/14425/PC11_PCA_Data_Highlights_Odisha](https://censusindia.gov.in/nada/index.php/catalog/11313/download/14425/PC11_PCA_Data_Highlights_Odisha.pdf)
678 .pdf
- 679 70. Liu F, Zhang X, Murayama Y, Morimoto T. Impacts of land cover/use on the urban thermal environment: A
680 comparative study of 10 megacities in China. *Remote Sens (Basel)* [Internet]. 2020;12(2):307. Available from:
681 <http://dx.doi.org/10.3390/rs12020307>
- 682 71. Guerri G, Crisci A, Messeri A, Congedo L, Munafò M, Morabito M. Thermal summer diurnal Hot-Spot analysis:
683 The role of local urban features layers. *Remote Sens (Basel)* [Internet]. 2021;13(3):538. Available from:
684 <http://dx.doi.org/10.3390/rs13030538>
- 685 72. Bounoua L, DeFries R, Collatz GJ, Sellers P, Khan H. Effects of land cover conversion on surface climate. *Clim*
686 *Change* [Internet]. 2002;52(1–2):29–64. Available from: <http://dx.doi.org/10.1023/a:1013051420309>
- 687 73. Halefom A, He Y, Nemoto T, Feng L, Li R, Raghavan V, et al. The impact of urbanization-induced land use
688 change on land surface temperature. *Remote Sens (Basel)* [Internet]. 2024;16(23):4502. Available from:
689 <http://dx.doi.org/10.3390/rs16234502>
- 690 74. Santamouris M, Synnefa A, Karlessi T. Using advanced cool materials in the urban built environment to mitigate
691 heat islands and improve thermal comfort conditions. *Sol Energy* [Internet]. 2011;85(12):3085–102. Available
692 from: <http://dx.doi.org/10.1016/j.solener.2010.12.023>
- 693 75. Al-huqail AA, Islam Z, Al-Harbi HF. Mangroves trend and their impact on surface temperature in Al-Wajh
694 Lagoon: a study aligned with Saudi Arabia’s vision 2030. *Front Environ Sci* [Internet]. 2024;12. Available from:
695 <http://dx.doi.org/10.3389/fenvs.2024.1439425>
- 696 76. Nanda D, Mishra DR, Swain D. COVID-19 lockdowns induced land surface temperature variability in mega
697 urban agglomerations in India. *Environ Sci Process Impacts* [Internet]. 2021;23(1):144–59. Available from:
698 <http://dx.doi.org/10.1039/d0em00358a>



- 699 77. Intergovernmental Panel on Climate Change (IPCC). Climate change 2022 – impacts, adaptation and
700 vulnerability: Working group II contribution to the sixth assessment report of the intergovernmental panel on
701 climate change [Internet]. Cambridge, England: Cambridge University Press; 2023. Available from:
702 <http://dx.doi.org/10.1017/9781009325844>
703



Data Availability

View Article Online
DOI: 10.1039/D6VA00012F

All satellite datasets used in this study are available on public domains. Field observations and codes can be made available on request to the corresponding author.

